land

MDPI

Article

Land Use Simulation and Identification of Core Carbon Sink Areas in the Beijing–Tianjin–Hebei Region

Ningyue Zhang [1,2], Yongqiang Cao [1,*], Jinke Wang [1,*], Xueer Guo [1] and Yiwen Xia [1]

[1] Academy of Eco-Civilization Development for Jing-Jin-Ji Megalopolis, Tianjin Normal University, Tianjin 300387, China; 2300080002@stu.tjnu.edu.cn (N.Z.); 2410080025@stu.tjnu.edu.cn (X.G.); 2510080029@stu.tjnu.edu.cn (Y.X.)
[2] Tianjin Urban Planning Compilation and Research Center, Tianjin 300201, China
* Correspondence: caoyongqiang@tjnu.edu.cn (Y.C.); 2410080019@stu.tjnu.edu.cn (J.W.)

Abstract

In the context of global climate change, the "dual carbon" goals, and land space planning, this study integrates the Patch-generating Land Use Simulation (PLUS) model, the Carnegie-Ames-Stanford Approach (CASA) model, and a soil respiration model (Heterotrophic Respiration, R_h) to simulate land use change and estimate Net Ecosystem Productivity (NEP) from 2002 to 2023. It projects the carbon sink pattern for 2030 using Hot Spot Analysis. The results show the following: (1) From 2020 to 2030, land use in the Beijing–Tianjin–Hebei region will be characterized by decreases in cropland and grassland and increases in impervious and forest, with cropland-to-impervious conversion dominating. (2) The spatial pattern of NEP exhibits a clear "high in mountainous areas and low in plains" distribution, where forest, grassland, and cropland function as carbon sinks, with forest having the strongest sequestration capacity. The carbon sink core areas cover approximately 59,479 km^2 and account for about 27.40% of the total area. (3) By 2030, the total carbon sink in the Beijing–Tianjin–Hebei region is projected to range from 31.81 to 32.39 Tg C under different scenarios, with forest contributing nearly 70%. The carbon sink core areas account for approximately 19.12–19.16 Tg C, representing about 60% of the total carbon sink.

Keywords: land space planning; land use; core carbon sink areas; optimized PLUS model; Beijing–Tianjin–Hebei region

1. Introduction

Climate change has become one of the most severe environmental challenges facing the world today. Controlling greenhouse gas emissions and advancing the goals of carbon peaking and carbon neutrality are crucial pathways towards achieving harmonious coexistence between humanity and nature [1,2]. At the seventy-fifth session of the United Nations General Assembly, China announced its commitment to striving for carbon dioxide emissions to peak before 2030 and endeavoring to achieve carbon neutrality before 2060. Research indicates that land use evolution influences regional ecological patterns and the spatiotemporal distribution of carbon sources/sinks [3,4], constituting one of the most direct anthropogenic drivers of terrestrial ecosystem carbon cycling [5]. Its impact ranks second only to fossil fuel combustion, with deforestation and the expansion of impervious surfaces being the primary causes of reduced carbon sink capacity [6]. Therefore, the rational identification of land use change patterns and the quantitative assessment of carbon budget dynamics are of paramount importance for coordinating the development

Check for updates

Academic Editor: Li Wang

Received: 14 March 2026
Revised: 21 April 2026
Accepted: 22 April 2026
Published: 24 April 2026

Copyright: © 2026 by the authors. Licensee MDPI, Basel, Switzerland. This article is an open access article distributed under the terms and conditions of the Creative Commons Attribution (CC BY) license.

and conservation of national territory, establishing an ecological security framework, and achieving the dual carbon goals.

Land space planning, as a key institutional framework for coordinating the governance of elements such as mountains, waters, forests, cropland, lakes, grasslands, and desert areas, has progressively become the core instrument for regulating land use patterns, balancing resource–environmental carrying capacity and spatial development intensity. Land use directly reflects the evolution of land space patterns and serves as a key driver of ecosystem services and carbon cycle dynamics. In recent years, research employing land use simulation models has advanced rapidly both domestically and internationally. Among these, the PLUS model has gained widespread application in regional land use change simulations due to its strengths in preserving landscape patterns, enabling spatially adaptive partitioning, and facilitating multi-scenario projections. It effectively captures the trajectory of land use evolution [7,8]. However, existing research predominantly remains confined to holistic simulation frameworks driven by comprehensive factors, lacking a disaggregated analysis of natural and societal driving forces. Consequently, it proves challenging to elucidate the relative contributions of different drivers within land use change dynamics. When employing the PLUS model for forecasting, most scholars fail to incorporate national spatial control policies such as the "Three Zones and Three Lines" framework. This omission may introduce deviations in simulation outcomes concerning policy constraints and planning orientations.

Concurrently, research on land use change has progressively expanded into the domains of carbon cycling and carbon sink functionality assessment. NEP, serving as a core metric for evaluating ecosystem carbon source/sink status, systematically reflects the contributions to and constraints of different land use types in terms of carbon cycling, thereby providing crucial quantitative evidence for spatial pattern optimization. Currently, NEP calculation methods are relatively well-established. The remote sensing data-driven CASA model has been widely applied for estimating regional-scale NPP, with NEP values derived by integrating soil respiration (R_h) processes [9,10]. From the perspective of land space governance practice, the current delineation and regulatory framework for ecological conservation red lines is mainly centered on key ecological functions such as water conservation, biodiversity maintenance, soil and water conservation, windbreak and sand fixation, and coastal ecological stability, as well as ecologically sensitive and fragile areas. Although carbon sequestration is closely related to ecological security and the enhancement of ecosystem services, it has not yet been explicitly incorporated as a core basis for delineation on a par with the functions above [11]. Against the backdrop of implementing the "three zones and three lines" policy, the existing system still places primary emphasis on the strict control of the spatial boundaries of ecological conservation red lines and of development activities within them, while more direct quantitative support remains lacking for how the identification of core carbon sink areas can be embedded into land space optimization, the prioritization of ecological restoration, and governance oriented towards carbon sequestration enhancement. This has resulted in the relative neglect of the interaction between land use change and carbon budgets in land space planning, making it difficult to strengthen regional carbon sequestration potential through optimized spatial arrangements [12–14]. This has resulted in a relative absence of consideration for the interplay between land use change and carbon budgets within land space planning frameworks, making it challenging to enhance regional carbon sequestration potential through optimized spatial arrangements.

The Beijing–Tianjin–Hebei region, located in the heart of North China and the core area surrounding the Bohai Sea, serves as an important ecological barrier in northern China, a major grain-producing region, and a key economic growth pole. It is also a typical

region characterized by rapid urbanization, intense land use change, and pronounced conflicts between carbon sources and sinks. The regional landscape broadly follows a "north-western mountains and hills–south-eastern plains and coastal zone" pattern, with forests, grasslands, and cropland as the dominant vegetation and land-cover types, and with marked differences in topography and land use structure [15]. Relevant studies have shown that land use change in the Beijing–Tianjin–Hebei region is mainly characterized by the expansion of impervious and the reduction in cropland. Impervious constitutes the principal source of carbon emissions, whereas forest is the most important carbon sink carrier. Spatially, carbon emissions generally display a pattern of "higher in the south-east and lower in the north-west", with high-carbon-source areas concentrated in Beijing, Tianjin, and the more intensively developed coastal and plain areas, while Chengde, Zhangjiakou, and the Yanshan–Taihangshan ecological conservation zone function as important carbon sink areas [16]. At the same time, Beijing, Tianjin, and Hebei differ markedly in their low-carbon transition trajectories: Beijing has largely completed its shift towards a low-carbon industrial structure and is at a relatively advanced stage; Tianjin remains in the climbing phase towards carbon peaking under a manufacturing-led economy; and Hebei, constrained by its high proportion of heavy industry and strong energy intensity, faces more prominent pressures for both emission reduction and sink enhancement [17]. The Beijing–Tianjin–Hebei region is, therefore, not only a representative area for examining how land use change affects regional carbon sink functions, but also a key region for exploring differentiated pathways for sink enhancement and coordinated regional governance.

In summary, existing studies have developed relatively mature theories and methods for land use simulation and carbon budget assessment. However, research on the decomposition of driving factors of land use change and multi-scenario simulations remains insufficient, and land space planning policies have not been fully incorporated into the PLUS model. As a result, the linkage between regional carbon sequestration potential and spatial optimization is still inadequate. In light of this, this study selected the Beijing–Tianjin–Hebei region as the study area, integrated multi-source data, and coupled an optimized PLUS model with the CASA–R_h framework to achieve the integration of land use change simulation and net carbon sink assessment at the regional scale. An integrated "land use–carbon sink" analytical framework was thus established. A Hot Spot Analysis method was introduced to identify carbon sink core areas and to quantitatively characterize the spatial clustering patterns of carbon sinks. Furthermore, by incorporating multi-scenario simulations, the response characteristics and evolutionary trends of carbon sink patterns under different development pathways were analyzed to provide scientific support and decision-making references for constructing a land space development and protection pattern oriented towards enhanced carbon sequestration.

2. Materials and Methods

2.1. Study Area

The Beijing–Tianjin–Hebei region lies in the transition zone between the North China Plain and the mountainous areas (113°27′–119°50′ E, 36°05′–42°40′ N). As the core area of China's capital economic circle and the Bohai Rim region, it comprises the municipalities of Beijing and Tianjin, along with 11 prefecture-level cities in Hebei Province, covering a total area of approximately 217,000 km^2. The administrative divisions and topography of the study area are depicted in Figure 1.

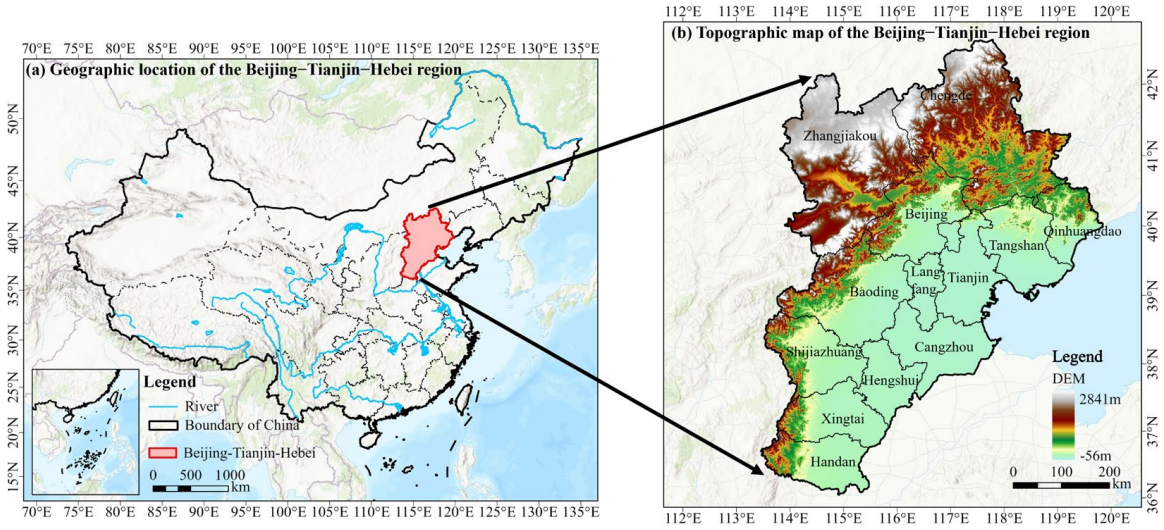


Figure 1. General map of the study area. (**a**) Geographic location of the Beijing–Tianjin–Hebei region, (**b**) topographic map of the Beijing–Tianjin–Hebei region. Note: DEM is Digital Elevation Model.

2.2. Data Sources

This study integrates multi–source data (Table 1), which were harmonized through resampling to a common spatial resolution and temporal scale, and standardized to the EPSG: 3857 coordinate system with a spatial resolution of 500 m × 500 m. The carbon emissions data represent fossil CO_2 emissions, encompassing all fossil CO_2 sources, with other greenhouse gases excluded [18]. In terms of temporal selection, long–term datasets covering 2002–2023 were used to characterize historical dynamics and trend patterns, whereas single–year datasets were adopted as driving factors in the PLUS model. Considering the historical simulation period (2010–2020) and the temporal step settings of the PLUS model, the driving factor data were selected from the year 2020 [19].

Table 1. Data types and sources.

Data	Spatial Resolution	Unit	Sources	Time
Land Use Type	30 m	—	Earth System Science Data (https://zenodo.org/records/12779975, accessed on 15 September 2025)	2002–2023
Net Primary Productivity (NPP)	500 m	gC/m^2	MODIS (MOD17A3HGF, NPP)	2002–2023
Normalized Difference Vegetation Index (NDVI)	500 m	—	MODIS (MOD09GA, sur_refl_b01, sur_refl_b02)	2002–2023
Temperature	4638.3 m	°C	TerraClimate (tmmn, tmmx)	2002–2023
Precipitation	4638.3 m	mm	TerraClimate (pr)	2002–2023
Solar Radiation	4638.3 m	W/m^2	TerraClimate (srad)	2002–2023
Terrestrial Water	0.5°	Equivalent water height	National Tibetan Plateau Data Center (http://data.tpdc.ac.cn, accessed on 15 September 2025)	2020
Groundwater	0.5°	Equivalent water height	National Tibetan Plateau Data Center (http://data.tpdc.ac.cn, accessed on 15 September 2025)	2020
Night Light	15″ (About 500 m)	Light intensity	National Earth System Science Data Center (https://www.geodata.cn, accessed on 15 September 2025)	2020

Table 1. *Cont.*

Data	Spatial Resolution	Unit	Sources	Time
Digital Elevation Model (DEM)	30 m	m	WorldDEM (https://space-solutions.airbus.com/imagery/3d-elevation-and-reference-points/worlddem-neo, accessed on 15 September 2025)	—
Slope	30 m	°	Using DEM data, the calculation was performed in ArcGIS 10.5. Slope is used to characterize the steepness of terrain, which affects land use suitability and vegetation distribution.	—
Slope Aspect	30 m	—	Using DEM data, the calculation was performed in ArcGIS 10.5. Slope aspect reflects the orientation of the land surface and significantly impacts solar radiation reception and microclimate conditions.	—
Terrain Undulation	30 m	°	Using DEM data, the calculation was performed in ArcGIS 10.5.	—
Gross Domestic Product (GDP)	1000 m	Ten thousand yuan	https://github.com/thestarlab/ChinaGDP, accessed on 15 September 2025	2020
Population	30″ (about 1000 m)	Person	LandScan (https://landscan.ornl.gov, accessed on 15 September 2025)	2020
Distance from Points of Interest (POI)	—	m	Using data from the Open Street Map, calculate the Euclidean distance in ArcGIS to obtain. It represents the distance of each pixel to the nearest point of interest (including commercial facilities, residential areas, and public service facilities), used to characterize the intensity of human activity and spatial accessibility.	2020
Distance from roads	—	m	Using data from the Open Street Map, calculate the Euclidean distance in ArcGIS 10.5 to obtain	2020
Distance from railways	—	m	Using data from the Open Street Map, calculate the Euclidean distance in ArcGIS 10.5 to obtain	2020
Distance from Impervious	—	m	Using data from the Science Data Bank, calculate the Euclidean distance in ArcGIS 10.5 to obtain	2020
CO_2 Emission	0.1°	tCO_2	EDGAR—Emissions Database for Global Atmospheric Research (https://edgar.jrc.ec.europa.eu/, accessed on 15 September 2025)	2020

2.3. Methodology

To enhance the interpretability of the results and the completeness of process representation, this study developed an integrated "land use–carbon sink" simulation framework by coupling the PLUS, CASA, and Rh models. The PLUS model simulates the spatial expansion and transition of land use under multiple driving factors, providing strong spatially explicit modeling capability. The CASA model, based on light use efficiency theory, estimates vegetation net primary productivity (NPP) using remote sensing data and is suitable for regional-scale carbon uptake simulation. The Rh model characterizes soil heterotrophic respiration from a climate-driven perspective and represents ecosystem carbon release fluxes.

By integrating these models, the framework enables an explicit linkage between land use change and carbon sink dynamics, while simultaneously accounting for both natural and socio-economic drivers in scenario simulations, thereby improving the comprehensiveness and reliability of regional carbon source/sink assessments.

2.3.1. Land Use Simulation Methods

(1) Markov Model

The land use transition matrix is generated by assigning state transition probabilities to the quantities or proportions of land area converted between land use types. This enables quantitative analysis of temporal changes in land use types, revealing their structural characteristics and evolving trends [20]. The calculation formula is presented in Equation (1):

$$S_{ij} = \begin{bmatrix} S_{11} & S_{12} & \dots & S_{1n} \\ S_{21} & S_{22} & \dots & S_{2n} \\ \vdots & \vdots & \vdots & \vdots \\ S_{n1} & S_{n2} & \dots & S_{nn} \end{bmatrix} \quad (1)$$

where n denotes the number of land categories; i and j represent the initial land categories at the start of land conversion during the study period, respectively ($i, j = 1, 2, \dots, n$); S_{ij} denotes the conversion area between land categories i and j.

(2) PLUS Model

The PLUS model primarily comprises two main modules: the land expansion analysis strategy (LEAS) and the cellular automata model based on multi-type random seeds (CARS) [21].

Land expansion analysis strategy (LEAS): By comparing land use data across two time periods, this approach identifies expansion areas for various land categories and employs a random forest algorithm to quantify the contribution of each driving factor to land change [22]. This paper decomposes driving factors into natural and social components. Natural factors comprise: digital elevation model (DEM), slope gradient, slope aspect, terrain undulation, air temperature, precipitation, terrestrial water, and groundwater storage. Social factors include GDP, night light, population density, distance to points of interest (POI), distance to roads, distance to railways, distance to built-up areas, and carbon dioxide emissions. By conducting LEAS analyses using natural factors, social factors, and all drivers respectively, the driving effects of individual factor groups on various types of land expansion can be determined. These results can then be compared with the full-driver analysis to identify the relative contributions of natural and social factors to land expansion, revealing their heterogeneous driving characteristics in the spatial distribution of land use.

A cellular automata model based on multi-class random patch seeds (CARS): Building upon the CA model framework, this approach employs random seed generation and a threshold reduction mechanism, integrated with developmental probability constraints, to

achieve spatio-temporal dynamic simulation of land patches. During simulation, neighborhood weights reflect the conversion rates and expansion capacities between different land categories. Neighborhood weight parameters range from 0 to 1, with values closer to 1 indicating stronger expansion capabilities [23]. This paper employs a Markov model to forecast future landscape type demand. Based on the land use transition matrix for the study area from 2010 to 2020, the neighborhood weights undergo iterative adjustment, ultimately selecting the parameter combination yielding the highest precision [24] (Table 2). The accuracy of simulation results is assessed using the Kappa coefficient, which ranges from 0 to 1. A value exceeding 0.7 indicates a high degree of accuracy in the simulation results [25].

Table 2. Neighborhood weight parameters.

Land Use Types	Cropland	Forest	Grassland	Water	Barren	Impervious
Neighborhood weights	0.2041	0.2789	0.1129	0.0372	0.0001	0.3668

Optimization of spatial expansion probability data: The expansion probability data within the PLUS model quantifies regional land spatial expansion patterns, playing a crucial role in future land use simulations. Drawing upon the research of scholars such as Li Peiyao [26], this paper selects the three control lines with the greatest impact on land use within the Beijing–Tianjin–Hebei regional spatial planning framework—the ecological conservation red line, the permanent basic cropland protection red line, and the city development boundary—to optimize the expansion probability raster for land use types. An expansion probability of 0 indicates that the land type in that area is unlikely to expand, while an expansion probability of 1 indicates that the area is prioritized for expansion. The optimization rules are shown in Table 3.

Table 3. Optimization rules for land use expansion probability.

Policy Type	Optimization Rule
Ecological Conservation Red Line	Probability of expanding cropland and impervious within the Ecological Conservation Red Line is 0
Permanent Basic Cropland Protection Red Line	Probability of expanding cropland within the Permanent Basic Cropland Protection Red Line is 1
City Development Boundary	Probability of expanding impervious within the City Development Boundary is 1

2.3.2. Carbon Source/Sink Modeling Methods

(1) CASA Model

In 1972, scholars, including Potter [27], jointly proposed the CASA model, a parameterized model for photosynthetic energy use efficiency based on Monteith's equations. The primary parameters simulating NPP within this model are the absorbed photosynthetically active radiation ($APAR$) and the actual photosynthetic energy use efficiency (ε). The calculation formula is presented in Equation (2):

$$NPP(x,t) = APAR(x,t) \times \varepsilon(x,t) \quad (2)$$

where $NPP(x,t)$ denotes the cumulative NPP value ($gC \cdot m^{-2} \cdot t^{-1}$) for pixel x over time t, $APAR(x,t)$ represents the photosynthetically active radiation absorbed by pixel x during time t ($MJ \cdot m^{-2} \cdot t^{-1}$), and $\varepsilon(x,t)$ indicates the actual photosynthetic efficiency ($gC \cdot MJ^{-1}$) for

pixel x at time t. In this equation, the calculation of $APAR$ is determined by two variables: the fractional photosynthetically active radiation ($FPAR$) and the solar total radiation (SOL). The calculation formula is presented in Equation (3):

$$APAR(x,t) = SOL(x,t) \times FPAR(x,t) \times 0.5 \tag{3}$$

where $SOL(x,t)$ denotes the total solar radiation (MJ·m^{-2}·t^{-1}) received by pixel x during time interval t, while $FPAR(x,t)$ represents the proportion of photosynthetically active radiation absorbed by pixel x. The value 0.5 indicates the proportion of total solar radiation utilized for photosynthesis. The photosynthetic energy use efficiency is simultaneously influenced by external environmental factors such as air temperature and precipitation, thereby affecting the value of vegetation NPP. The calculation formula is presented in Equation (4):

$$\varepsilon(x,t) = \varepsilon_{\max} \times Stress(x,t) \tag{4}$$

where $Stress(x,t)$ denotes the stress coefficient reflecting the impact of air temperature and precipitation on photosynthetic efficiency, while $\varepsilon_{\max}$ represents the maximum photosynthetic efficiency achievable under ideal conditions. The parameter values for each land use category in this study draw upon those established in Zhu Wenquan's prior research [28].

(2) R_h Model

Employing the ecosystem heterotrophic respiration (soil) calculation model established by Odum [29] based on field measurements, this model estimates carbon emissions from soil microbial respiration using air temperature and precipitation data. The calculation formula is presented in Equation (5):

$$R_h(x,t) = 0.22 \times (\exp(0.0912T(x,t)) + \ln(0.3145P(x,t) + 1)) \times 30 \times 46.5\% \tag{5}$$

where $R_h(x,t)$ denotes the carbon released by soil microbial respiration at pixel x at time t (gC·m^{-2}·t^{-1}), $T(x,t)$ represents the average air temperature at pixel x at time t (°C), and $P(x,t)$ indicates the average precipitation at pixel x at time t (mm).

(3) Carbon Source/Carbon Sink (NEP) Calculation

Net ecosystem productivity refers to the portion of net primary productivity after subtracting the respiratory output of heterotrophic organisms within the ecosystem (soil respiration) [30]. The calculation formula is presented in Equation (6):

$$NEP(x,t) = NPP(x,t) - R_h(x,t) \tag{6}$$

where $NEP(x,t)$ denotes the net ecosystem productivity (gC·m^{-2}·t^{-1}) of pixel x at time t, $NPP(x,t)$ denotes the net primary productivity (gC·m^{-2}·t^{-1}) of pixel x at time t, and $R_h(x,t)$ denotes the ecosystem heterotrophic respiration (gC·m^{-2}·t^{-1}) of pixel x at time t.

2.3.3. Spatial Autocorrelation Analysis (Global Moran's I)

To analyze the spatial clustering characteristics of NEP, this study employs the Global Moran's I statistic to test spatial autocorrelation. The calculation formula [31] is presented in Equation (7):

$$I = \frac{n}{\sum_{i=1}^{n}\sum_{j=1}^{n} w_{ij}} \cdot \frac{\sum_{i=1}^{n}\sum_{j=1}^{n} w_{ij}(x_i - \bar{x})(x_j - \bar{x})}{\sum_{i=1}^{n}(x_i - \bar{x})^2} \tag{7}$$

where n denotes the number of spatial units; x_i and x_j represent the observed values of the i-th and j-th spatial units, respectively; $\bar{x}$ is the mean value; and w_{ij} is the spatial weight matrix. The estimation of Moran's I may be influenced by factors such as spatial heterogeneity, data resolution, and scale effects, which could lead to deviations.

2.3.4. Identification of Carbon Sink Reserves Based on Hot Spot Analysis

Spatial clustering analysis methods can quantitatively reflect the spatial distribution patterns of certain elements, thereby facilitating the implementation of centralized, targeted management measures [32]. This study employs Hot Spot Analysis within spatial clustering methodologies to identify carbon sink conservation areas. The Hot Spot Analysis utilizes the Getis–Ord G* index, a local association measure proposed by British mathematician Getis et al. in 1992, for its analysis [33]. Based on the Getis–Ord Gi* statistic, a local clustering test was conducted on 500 m resolution NEP grids. Employing the Benjamini–Hochberg method to control the false discovery rate ($\alpha = 0.05$) at the pixel-level multiple testing stage, significantly positive clustering zones ($Z > 0$ and passing FDR-BH) were overlaid with the NEP > 0 condition to identify carbon sink conservation areas. Spatial filtering was then applied with a minimum contiguous threshold of 10 km^2. The Getis–Ord Gi* calculation formula is presented in Equation (8):

$$G_i^* = \frac{\sum_{j=1}^{n} \omega_{i,j} x_j - \bar{X} \sum_{j=1}^{n} \omega_{i,j}}{S \sqrt{\frac{n \sum_{j=1}^{n} \omega_{i,j}^2 - \left(\sum_{j=1}^{n} \omega_{i,j} \right)^2}{n - 1}}} \tag{8}$$

where x_j denotes the attribute value of factor j, $\omega_{i,j}$ represents the spatial weight between factors i and j, n is the total number of factors, $\bar{X}$ is the mean value of all factor attribute values, and S is the standard deviation of the attribute values. The calculation formula is presented in Equations (9) and (10):

$$\bar{X} = \frac{\sum_{j=1}^{n} x_j}{n} \tag{9}$$

$$S = \sqrt{\frac{\sum_{j=1}^{n} x_j^2}{n} - \bar{X}^2} \tag{10}$$

where G_i^* statistic returned for each element constitutes the z-score. For positive z-scores of statistical significance, the higher the z-score, the more tightly clustered the high-value elements.

3. Results

3.1. Land Use Simulation

3.1.1. Verification of Land Use Simulation Accuracy

Based on 2010 land use data, the simulated 2020 land use data was validated against the current 2020 land use status (Figure 2). The Kappa coefficient of 0.89 (according to relevant standards [19], when the Kappa coefficient exceeds 0.75, the model may be deemed to possess reliable predictive capability) indicates that the PLUS model's simulation results possess a high degree of reliability.

3.1.2. Future Land Use Projections and Decomposition of Driving Factors

To investigate the driving effects of natural and socio-economic factors on the expansion of different land use types during land use change, and to compare them with the results driven by all factors, three sets of driving factors were inputted into the LEAS module for analysis. The contribution of each driving factor was quantified using feature importance derived from the random forest model. Subsequently, the CARS module was applied to simulate land use change, and the land use transition areas (Table 4) and spatial patterns (Figure 3) for 2030 under natural, socio-economic, and combined driving scenarios were simulated and projected.

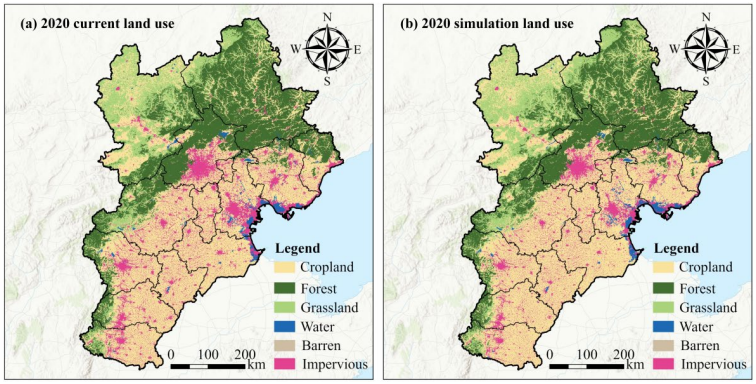


Figure 2. Comparison of current and simulation land use data in the Beijing–Tianjin–Hebei region in 2020. (**a**) 2020 current land use; (**b**) 2020 simulation land use.

Table 4. Projected land use transfer area driven by natural factors, social factors, natural and social factors from 2020 to 2030.

Transfer Type	Area/km^2		
	Natural Factors	Social Factors	Natural and Social Factors
Cropland → Forest	130.50	223.50	92.50
Cropland → Impervious	4305.75	4212.75	4343.75
Grassland → Forest	2771.50	2670.75	2809.00
Grassland → Impervious	1190.75	1231.25	906.50
Water → Forest	0.25	8.00	0.75
Water → Impervious	74.00	66.25	73.50
Barren → Grassland	0.50	1.50	1.25
Barren → Impervious	4.00	5.25	3.25
Impervious → Grassland	84.00	22.75	31.75

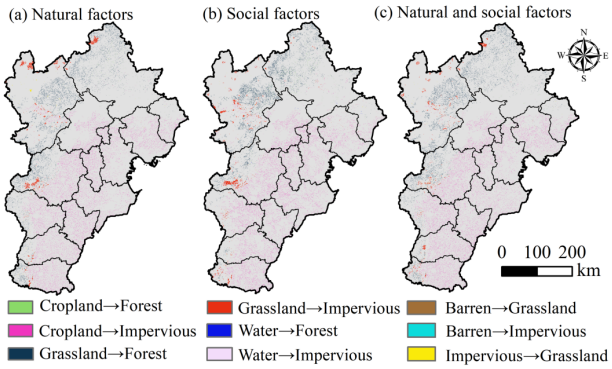


Figure 3. Projected distribution of land use transfer driven by by different factors from 2020 to 2030. (**a**) Natural factors. (**b**) Social factors. (**c**) Natural and social factors.

In this study, the land use pattern in 2020 was adopted as the initial state for the simulation, and the land use pattern in 2030 was simulated and projected based on historical land use evolution patterns, thereby providing a consistent baseline for comparing different driving factor groups. The transition areas reported in Table 4 represent the land use changes simulated under different driving mechanisms from the same initial condition and were used to characterize the differences in land use dynamics among the driving factor groups.

In terms of area, the land use conversion within the Beijing–Tianjin–Hebei region during the simulation period from 2020 to 2030 exhibits distinct typological variations and factor-dependent characteristics. Among these, cropland-to-impervious conversion represents the largest area, with the three driving factor groups showing transition areas of 4305.75 km^2, 4212.75 km^2, and 4343.75 km^2, respectively. This simulated and projected transformation process reflects the trend of cropland reduction and impervious expansion

during urbanization. The conversion of grassland to forest and impervious also exhibits a considerable scale, reflecting a parallel trend of ecological restoration and development demands. The conversion areas for water and barren were relatively small in the simulation results, indicating that these land types possess limited conversion potential under natural conditions and social management.

From the perspective of differences among the three driving factors, the area of cropland converted to forest under social factors is simulated and projected to be 223.5 km^2, significantly exceeding that driven by natural factors or all factors combined. This phenomenon indicates that, during the simulation period, the spatial distribution of forests is primarily driven by social factors, notably population density (contribution 0.18), CO_2 emissions (contribution 0.17), and spatial expansion pressures (including distance from built-up areas, roads, railways, points of interest, and GDP, with combined contributions exceeding 0.6). As shown in Figure 3, the conversion of cropland to forest mainly occurs in mountainous regions during the simulation period. These areas, characterized by challenging development conditions, sparse populations, and low agricultural returns, possess significant vegetation restoration potential. Consequently, under policy guidance, they are more conducive to implementing the Grain-for-Green Project, forming stable carbon sinks that positively support the overall carbon surplus pattern. The area of impervious surface converted to grassland under natural factors is simulated and projected to be 84 km^2, significantly higher than that driven by social factors or all factors combined, demonstrating a pronounced natural driver effect. Among these, annual mean air temperature (contribution 0.31), precipitation (contribution 0.15), slope (contribution 0.12), and terrain undulation (contribution 0.13) indicate that grassland is readily restored in non-plains areas with suitable air temperatures and adequate rainfall. As shown in Figure 3, the areas where impervious surfaces converted to grassland are mainly located in the Bashang region of Zhangjiakou City during the simulation period, which is suitable for grassland expansion.

In terms of patch distribution, during the simulation period, the area of grassland converted to impervious surfaces, though not significantly different in numerical terms, is primarily driven by natural factors in the patches located in the northern parts of Chengde and Zhangjiakou (Figure 3). Among these, slope (contribution 0.22), terrain undulation (contribution 0.22), and DEM (contribution 0.21) were the principal drivers. Despite relatively higher elevations, the terrain in northern Chengde and Zhangjiakou is relatively flat with minimal terrain undulation, rendering it suitable for impervious surface development.

3.1.3. Simulation of Future Land Use Scenarios

To explore land use evolution under different development objectives in the study area, four scenarios—baseline, urban development, ecological development, and comprehensive development—were established based on observed land use change characteristics, spatial planning policies, and relevant studies [34]. The baseline scenario was dominated by historical trends and maintained the natural trajectory of land use change, serving as a reference for policy-oriented scenarios.

The urban development scenario prioritized economic growth, population expansion, and accelerated urbanization, emphasizing the shift in land resources toward economic uses. Following Li Chen et al. [35], and based on the baseline scenario, the conversion of cropland and impervious to other types was restricted, while the transition probabilities from forest, grassland, and barren to impervious were increased by 20%, and those from forest and grassland to cropland were also increased by 20%, to strengthen the support of impervious and agricultural space for economic growth and population-carrying capacity.

The ecological development scenario prioritized ecological land types such as forest, grassland, and water, emphasizing the enhancement of carbon sequestration capacity through land use structure optimization. Based on the baseline scenario, the conversion probabilities from forest and grassland to impervious and barren were reduced by 20%, while the transition probabilities from barren to forest and grassland were increased by 20%, thereby promoting ecological expansion and suppressing the uncontrolled growth of high-emission impervious.

The comprehensive development scenario aimed to balance urban development needs with carbon reduction and efficiency improvement through optimized land resource allocation. Based on the baseline scenario, the transition probabilities from barren to cropland, forest, grassland, water, and impervious were increased by 20%; the transition probabilities from impervious to all land types except cropland were reduced by 20%; and the conversion probabilities from forest and grassland to impervious and barren were reduced by 20%, guiding land use toward structural optimization and efficiency enhancement.

The simulation results indicate significant differences in land use structure among scenarios. Under the baseline scenario, cropland was 94,507.25 km^2, forest was 61,139.5 km^2, grassland was 25,423.75 km^2, water were 2559 km^2, barren was 5 km^2, and impervious was 32,160.75 km^2, reflecting the continuation of historical patterns.

Under the urban development scenario, cropland increased to 95,075 km^2, showing a slight rise compared with the baseline, indicating stable agricultural space. Forest decreased to 60,885.75 km^2, grassland slightly increased to 25,467 km^2, water decreased marginally to 2558.25 km^2, barren remained at 5 km^2, and impervious decreased to 31,804.25 km^2. This suggests that, while restricting the uncontrolled expansion of impervious, part of the forest was converted to achieve coordinated adjustment between agricultural and urban spaces.

Under the ecological development scenario, cropland increased significantly to 97,730.25 km^2, the highest among all scenarios. Forest was 61,138.25 km^2, remaining close to the baseline level with a slight decrease. Grassland increased substantially to 27,873.5 km^2, water expanded to 2633.25 km^2, barren remained at 5 km^2, and impervious decreased markedly to 26,415 km^2. These results indicate that the ecological protection orientation effectively promoted the expansion of grassland and water while significantly reducing impervious, thereby enhancing regional carbon sink potential.

Under the comprehensive development scenario, cropland was 94,546 km^2 and forest was 61,136.25 km^2, both close to baseline levels with minor changes. Grassland increased to 26,295.75 km^2, water decreased to 2522.25 km^2, barren slightly increased to 5.75 km^2, and impervious was 31,289.25 km^2, lower than the baseline but higher than in the ecological scenario. This reflects a balanced approach that meets development needs while moderately controlling impervious expansion (Figure 4).

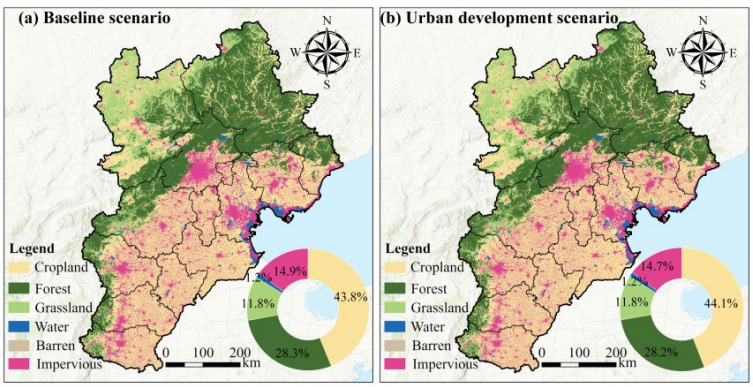


Figure 4. *Cont.*

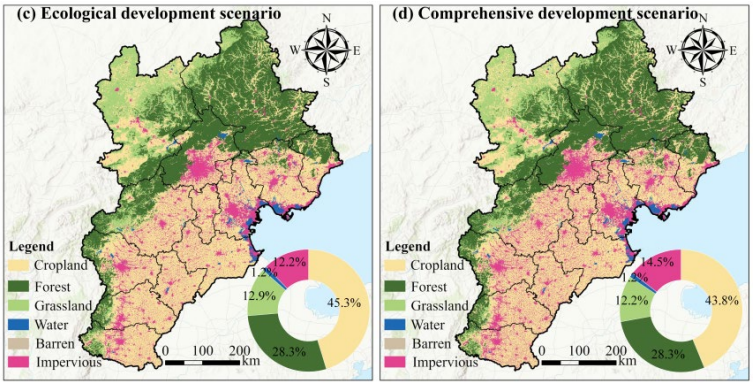


Figure 4. Projected land use patterns in the Beijing–Tianjin–Hebei region under different scenarios in 2030. (**a**) Baseline scenario, (**b**) urban development scenario, (**c**) ecological development scenario, and (**d**) comprehensive development scenario.

3.2. Carbon Source/Sink Modeling

3.2.1. Verification of NPP Simulation Accuracy

NPP simulations may exhibit systematic errors in model construction, parameterization, spatial resolution, and data quality, coupled with limited observational data. This study compared and validated the CASA model-simulated NPP with MOD17A3HGF NPP. Numerically, 1000 random sample points were selected within the study area to validate the annual mean NPP values for both models over 2002–2023. Results indicate a coefficient of determination (R^2) of 0.60, demonstrating satisfactory fitting performance (Figure 5). Regarding spatial distribution, Moran's I index was applied to evaluate the annual averages from 2002 to 2023. The index value reached 0.96, indicating consistent spatial patterns between the two datasets. Consequently, the simulated NPP results in this study demonstrate high reliability.

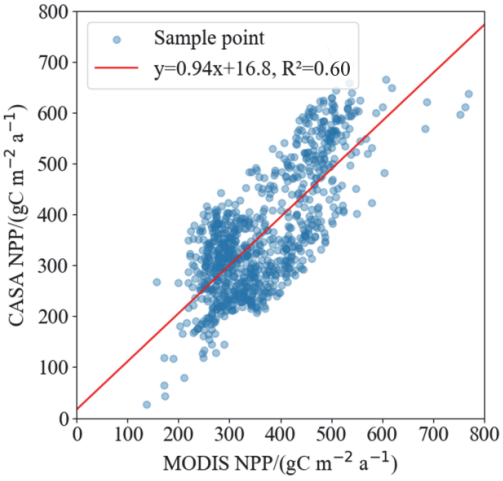


Figure 5. Comparison and verification results of simulated NPP and MODIS data.

3.2.2. Analysis of Spatiotemporal Distribution and Carbon Sequestration Rate Characteristics of NEP

The spatial distribution and trend of annual mean NEP in the Beijing–Tianjin–Hebei region from 2002 to 2023 are shown in Figure 6. Overall, the annual mean NEP ranged between −285.26 and 740.84 gC m^{-2} a^{-1}, exhibiting significant spatial variation. Influenced by topography and climate, the western Taihang Mountains and northern Yanshan Mountains, with their extensive vegetation cover, formed high-value zones distributed along the mountain ranges. Conversely, the eastern and southern plains exhibited low-value zones, with scattered clusters of low values concentrated in the built-up areas of Beijing, Tianjin,

and several cities in Hebei Province. Using the least squares method to calculate slopes and analyze trends, it was found that NEP showed an increasing trend across most of the Beijing–Tianjin–Hebei region. Conversely, NEP decreased around the main urban areas of Beijing, within the main urban areas of Tianjin and along the Bohai Bay coastline, as well as within the urban areas of various prefecture-level cities.

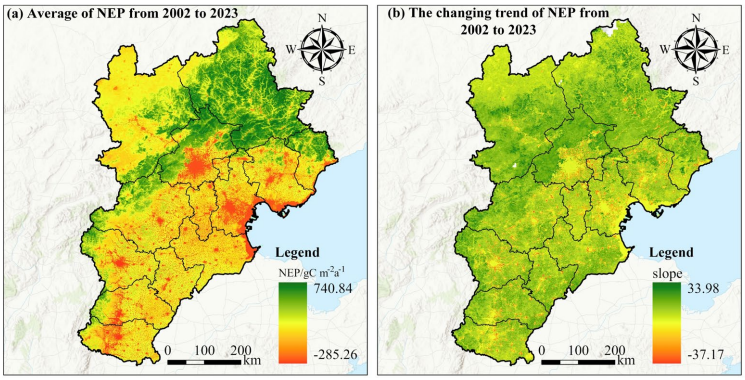


Figure 6. Temporal and spatial distribution changes in NEP in the Beijing–Tianjin–Hebei region from 2002 to 2023. (**a**) Average of NEP from 2002 to 2023. (**b**) The changing trend of NEP from 2002 to 2023.

To forecast the carbon sink distribution by 2030 and investigate the carbon sink capacity of different land use types, statistical analyses were conducted on the quartiles and mean values of each land use category from 2010 to 2023 (Figure 7). As the CASA model is primarily designed to simulate carbon processes in terrestrial vegetation ecosystems, where Net Primary Productivity (NPP) is driven by photosynthetic activity, water were retained within the spatial extent but excluded from NPP estimation in the CASA–based calculations [28], thereby ensuring both the completeness of regional analysis and the scientific consistency of the model application. Cropland, forest, and grassland all exhibit carbon sink attributes, though their sequestration levels and stability vary significantly. Among these, the forest exhibited the highest carbon sink rate, with an annual NEP of 360.91 gC m^{-2} a^{-1}, playing a pivotal role in the regional carbon sink. Grassland and cropland recorded annual NEP of 125.12 gC m^{-2} a^{-1} and 67.42 gC m^{-2} a^{-1}, respectively, also constituting crucial components in maintaining regional carbon balance. In contrast, impervious surfaces and barren exhibited typical carbon sink characteristics, with average annual NEP of −201.54 gC m^{-2} a^{-1} and −210.08 gC m^{-2} a^{-1}, respectively, indicating their significant carbon emission effects.

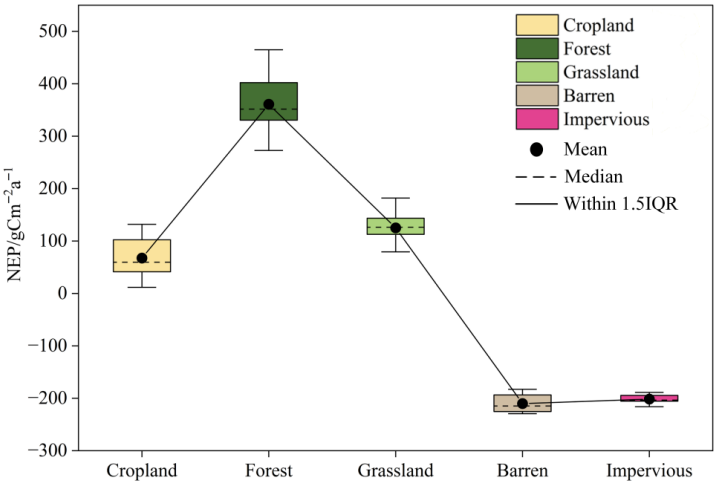


Figure 7. Distribution of annual mean NEP across terrestrial ecosystem types from 2010 to 2023. IQR denotes the Inter-Quartile Range.

3.3. Identification of Carbon Sink Core Areas and Future Carbon Sink Projections

3.3.1. Identification of Carbon Sink Core Areas

Using Hot Spot Analysis on NEP data from 2002 to 2023, high-value carbon sink clusters were identified (with a confidence level set above 95%) after excluding spatial units with zero values. The false discovery rate was controlled at $\alpha = 0.05$ (FDR–BH). Spatial overlay and merging analyses were conducted on the identified high-value carbon sink clusters from 2002 to 2023. Fragmented patches (area < 10 km^2) were excluded from the layers to ensure ecological functional continuity at the regional scale, ultimately yielding the spatial distribution of carbon sink core zones (Figure 8).

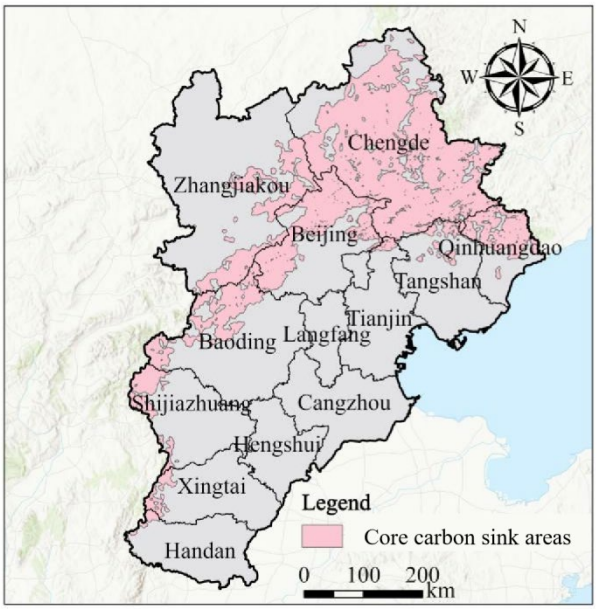


Figure 8. Spatial distribution of carbon sink core areas in the Beijing–Tianjin–Hebei region.

The core carbon sink areas are primarily situated in the northern Chengde, Qinhuangdao, Tangshan, and Tianjin; northwestern Beijing and Baoding; eastern Zhangjiakou; and western Shijiazhuang, Xingtai, and Handan. In terms of quantitative scale, the total area of identified carbon sink conservation zones amounts to 59,479.00 km^2, accounting for approximately 27.40% of the total land area within the Beijing–Tianjin–Hebei region.

3.3.2. Projected Carbon Sinks Under Future Multi-Scenario Land Use Patterns

Based on the land use area distribution for the Beijing–Tianjin–Hebei region in 2030 derived from Section 3.1.3, and the average annual carbon sequestration rates for carbon sink land use types in the region from 2010 to 2023 obtained from Section 3.2.2, the product of these two factors was calculated to determine the total carbon sink capacity for the Beijing–Tianjin–Hebei region and its core carbon sink areas in 2030 (Table 5).

By 2030, the overall variation in total carbon sequestration across different scenarios in the Beijing–Tianjin–Hebei region is projected to be relatively limited, whereas differences in source composition and structural patterns are more pronounced. Under the baseline scenario, total regional carbon sequestration is estimated at approximately 31.86 Tg C, with forest contributing the largest share (22.23 Tg C), accounting for about 69.77% of the total. Carbon sequestration from cropland and grassland is 6.39 Tg C and 3.24 Tg C, representing 20.06% and 10.17%, respectively. The carbon sink core area contributes 19.15 Tg C, accounting for 60.11% of the regional total, among which forest contributes as much as 96.08%, indicating its dominant role in sustaining the core carbon sink function.

Table 5. Carbon sink in the Beijing–Tianjin–Hebei region in 2030.

Scenario	Region	Total NEP in 2030 (Tg C)			
		Cropland	Forest	Grassland	Total
Baseline scenario	Beijing–Tianjin–Hebei region	6.39	22.23	3.24	31.86
	Core carbon sink areas	0.33	18.40	0.42	19.15
Urban development scenario	Beijing–Tianjin–Hebei region	6.43	22.14	3.24	31.81
	Core carbon sink areas	0.33	18.36	0.43	19.12
Ecological development scenario	Beijing–Tianjin–Hebei region	6.61	22.23	3.54	32.39
	Core carbon sink areas	0.32	18.40	0.44	19.16
Comprehensive development scenario	Beijing–Tianjin–Hebei region	6.40	22.23	3.35	31.97
	Core carbon sink areas	0.33	18.40	0.42	19.15

Under the urban development scenario, total regional carbon sequestration is estimated at 31.81 Tg C. Forest contributes 22.14 Tg C, accounting for approximately 69.60% of the total. Carbon sequestration from cropland and grassland is 6.61 Tg C and 3.24 Tg C, accounting for 20.21% and 10.19%, respectively. This indicates that the expansion of cropland provides a certain compensatory effect on carbon sequestration; however, due to the higher unit sequestration capacity of forest, its reduction still dominates the overall declining trend. The total carbon sequestration in the core area is 19.12 Tg C, with forest contributing 18.36 Tg C, further confirming the decisive role of forest changes in carbon sequestration.

Under the ecological development scenario, carbon sequestration shows the most significant increase, with a total of 32.39 Tg C. Forest contributes 22.23 Tg C, accounting for approximately 68.63% of the total. Carbon sequestration from cropland and grassland is 6.61 Tg C and 3.54 Tg C, accounting for 20.41% and 10.93%, respectively. Forest remains generally stable, while carbon sequestration from grassland and cropland increases. The total carbon sequestration in the core area is 19.16 Tg C, among which grassland contributes 0.44 Tg C, an increase of 0.01 Tg C compared with the baseline scenario, while forest and cropland remain stable.

Under the comprehensive development scenario, total regional carbon sequestration is estimated at 31.97 Tg C. Forest remains stable at 22.23 Tg C, accounting for approximately 69.53% of the total. Grassland carbon sequestration reaches 3.35 Tg C, an increase of 0.11 Tg C compared with the baseline scenario, while cropland remains generally stable, indicating that the increase in carbon sequestration is mainly attributed to structural optimization of grassland. The total carbon sequestration in the core area remains at 19.15 Tg C, consistent with the baseline scenario, and forest remains stable at 18.40 Tg C, reflecting the strong structural stability of the carbon sink system in the core area.

Overall, the carbon sink core area exhibits strong stability, and forest plays a crucial role in maintaining regional carbon sequestration functions. Although grassland has relatively limited sequestration capacity, it plays an irreplaceable role in enhancing carbon sink potential. cropland not only ensures food security but also provides carbon sequestration functions, demonstrating multiple ecological values. In the future, building on strengthened forest protection in core carbon sink areas, efforts should be made to promote the sustainable use and ecological restoration of cropland and grassland, to achieve a coordinated balance between ecological functions and regional development objectives.

4. Discussion

Existing studies generally indicate that, driven by urbanization, the Beijing–Tianjin–Hebei region has experienced continuous expansion of impervious and a persistent decline in cropland [36,37]. This conclusion is consistent with the dominant "impervious expansion–

cropland shrinkage" pathway identified in this study. The land use transition results of this study show that the conversion of cropland to impervious was the most significant among all transition types, indicating that impervious expansion remains the key force driving the reorganization of the regional land use pattern and continues to exert strong pressure on cropland resources. Meanwhile, previous research has also widely recognized that mountainous forest and grassland ecosystems play a strong carbon sequestration role, whereas plains and urbanized areas tend to function as carbon sources [38], which aligns with the "high in mountains–low in plains" spatial differentiation pattern of NEP revealed in this study's conclusion. The findings of this study, namely that forest exhibits the strongest carbon sequestration capacity, while grassland and cropland serve as important supplementary carbon sink components. In contrast, impervious and barren are characterized as carbon source types, further confirming the functional differentiation of carbon dynamics across land use types. In addition, studies on carbon sink spatial distribution have consistently highlighted strong spatial heterogeneity, emphasizing that key ecological spaces play a critical role in regional carbon cycling [39], which is also consistent with the carbon sink core areas identified in this study, mainly concentrated in the mountainous and hilly regions of northwestern Beijing–Tianjin–Hebei. This spatial pattern not only exhibits a high degree of overlap with high-NEP areas, but also further highlights the fundamental role of mountainous ecosystems in the formation of regional carbon sinks.

Most of existing studies have focused on carbon emissions or land use-based carbon budgets, emphasizing "where emissions are high" or "where carbon deficits are significant". In contrast, this study further characterizes regional net carbon sequestration capacity from the perspective of net ecosystem productivity (NEP), focusing on "which areas exhibit stable and concentrated carbon sink enhancement potential". This shift from "carbon emission identification" to "carbon sink core area identification" makes the results more relevant to land space optimization and ecological protection-oriented planning needs. Moreover, this study constructs an analytical framework of "land use simulation–NEP estimation–carbon sink core area identification". A clear transmission pathway was established between land use evolution processes and carbon cycle responses. Compared with previous studies, this study not only focuses on land use evolution, but also identifies and decomposes the effects of different driving factors. By examining the formation mechanisms underlying land use pattern evolution, it reveals the characteristics of spatial differentiation and thus provides a clearer basis for the setting of land use scenarios. On this basis, it simulates the land use pattern of 2030 under multiple scenarios and integrates land use scenarios under different development pathways with an assessment of regional carbon sink levels, thereby identifying potential future core carbon sink areas and their respective contributions. In this way, the study links land use scenario simulation with the spatial identification of regional carbon sinks. Compared with studies that focus solely on either land use prediction or static carbon accounting, this study places greater emphasis on the impacts of land use change on future carbon sink spatial patterns and attempts to translate these findings into a basis for land space planning optimization, thereby enhancing the linkage between model simulation results and planning applications.

The carbon assessment in this study is primarily based on net ecosystem productivity (NEP), which is determined by vegetation net primary productivity (NPP) and soil heterotrophic respiration (R_h). Therefore, the results mainly reflect the net carbon sequestration capacity dominated by vegetation processes. This characteristic is also reflected in the analysis of carbon sink differences among various land use types. However, spatial heterogeneity in vegetation structure and management practices exists within the same land use type, and differences in forest composition and management intensity may affect carbon storage capacity per unit area [40]. However, due to limitations in regional-scale

data availability and parameter standardization, such differences are represented using generalized land use-type parameters, which may, to some extent, reduce the precision of local-scale carbon sink estimation. Future studies could integrate high-resolution remote sensing data with forest inventory datasets to better parameterize vegetation structural heterogeneity and improve the spatial accuracy of carbon sink estimation. On the other hand, agricultural ecosystem carbon fluxes exhibit strong phenological sensitivity, with carbon uptake and release varying across growth stages [41]. However, this study conducted estimations at an annual scale, which integrates these temporal dynamics into averaged values. Future research could incorporate multi-temporal remote sensing data and crop growth models to explicitly represent phenological processes and improve the temporal resolution of cropland carbon cycle simulations. Furthermore, although NEP partially accounts for soil respiration through the inclusion of Rh, soil carbon pools themselves are characterized by long-term accumulation and turnover processes, and their coupling with vegetation carbon dynamics remains highly complex. In the current framework, these processes are represented in a simplified manner, and therefore the results primarily reflect vegetation-dominated net carbon uptake patterns. Future work could further incorporate soil organic carbon (SOC) and soil inorganic carbon (SIC) stocks and their dynamics, and is further supported by the carbon sink structural analysis presented in the Results section. This can be combined with multi-carbon-pool coupling models and anthropogenic disturbance processes (e.g., harvesting, land management, and logging activities), to achieve a more comprehensive representation of regional carbon storage and carbon cycling processes.

Based on the coupling analysis of land use change and carbon sink spatial patterns, at the spatial regulation level, process-based control of land use transitions should be strengthened through continuous monitoring and feedback optimization in combination with the land use change simulation results, using remote sensing and dynamic assessment methods. The “dynamic” aspect mainly refers to monitoring and management processes. Monitoring results derived from remote sensing inversion may be affected by spatial resolution, model parameterization, and input data quality, introducing certain uncertainties [42]. Therefore, in practical applications, ground-based observations or statistical data should be incorporated for validation and calibration to improve the reliability and accuracy of monitoring results. For rigid control boundaries such as permanent basic cropland, strict protection and stability constraints should be maintained, while achieving coordination between flexibility and rigidity in spatial governance. Moreover, carbon sink core areas are highly concentrated in mountainous forest systems, indicating strong spatial heterogeneity. Therefore, they should be incorporated into the land space ecological security pattern, with enhanced connectivity and stability of key ecological spaces. In key mountainous carbon sink regions, an ecological compensation mechanism based on carbon sequestration capacity and value orientation may be explored. Since NEP can represent regional carbon sink capacity, its spatial variation reflects, to some extent, the potential ecological value differences of regions under carbon neutrality targets and thus can serve as an important reference for ecological compensation design. Future studies may further introduce carbon market mechanisms, develop carbon sink valuation models, and explore pathways for converting carbon sink quantity into economic value, as well as its application in ecological compensation and spatial optimization, thereby improving the quantification and policy relevance of carbon sink management. Finally, carbon sink assessment results should be integrated into the land space planning system. Within the existing “three zones and three control lines” framework, carbon sink functional evaluation results can serve as an important reference for optimizing ecological protection redlines and conducting dynamic assessments, as well as for adaptive adjustment of land space patterns, thereby enhancing the support of planning implementation for the “dual carbon” goals.

5. Conclusions

This study focused on the Beijing–Tianjin–Hebei region and integrated multi-source remote sensing data and statistical information. An optimized PLUS model, the CASA model, and Hot Spot Analysis were employed to simulate future land use patterns, assess the evolution of carbon sources/sinks, and identify carbon sink core areas. The main conclusions are as follows:

(1) Land use evolution and driving mechanisms indicate that, from 2020 to 2030, the overall land use structure in the Beijing–Tianjin–Hebei region is projected to be characterized by a decrease in cropland and grassland and an increase in impervious and forest. Among these, cropland-to-impervious conversion exhibits the largest area, with transition areas of 4305.75 km^2, 4212.75 km^2, and 4343.75 km^2 for the three driving factor groups, respectively, forming a typical "imperious expansion–cropland loss" trajectory. The conversion from grassland to forest occurs at a considerable scale under the combined influence of natural and socio-economic factors, reflecting the potential for ecological restoration. In contrast, the transfer areas of water and barren are relatively small, indicating that their transitions are constrained by both natural conditions and policy regulations. The decomposition of driving factors shows that socio-economic factors play a more dominant role in the conversion from cropland to forest, with population, CO_2 emissions, and urban expansion pressure identified as the main drivers, while natural factors primarily control the restoration of impervious to grassland.

(2) The spatial pattern of carbon sources/sinks and the identification of carbon sink core areas indicate that from 2002 to 2023, NEP in the Beijing–Tianjin–Hebei region exhibits a clear "high in mountains–low in plains" spatial differentiation pattern. High-value carbon sink areas are mainly located in the Taihang Mountains in the west and the Yanshan Mountains in the north, while low-value areas are concentrated in the southeastern plains and coastal regions. Across land use types, forest, grassland, and cropland all function as carbon sinks, with forest showing the strongest carbon sequestration capacity, whereas impervious and barren act as carbon sources. Based on this, carbon sink core areas were identified, mainly distributed in the mountainous and hilly regions of the northwest, covering an area of approximately 59,479 km^2, accounting for 27.40% of the total regional area, indicating strong spatial heterogeneity.

(3) Multi-scenario carbon sink projections suggest that by 2030, total carbon sequestration in the Beijing–Tianjin–Hebei region will remain relatively stable across scenarios, ranging from 31.81 to 32.39 Tg C. Although overall variation is limited, significant differences in structure are observed, with the ecological development scenario showing the highest carbon sequestration level. Forest is the dominant contributor, accounting for nearly 70% across all scenarios, while grassland and cropland play important supplementary roles. Carbon sequestration in core areas remains stable between 19.12 and 19.16 Tg C, accounting for approximately 60% of the total regional carbon sink, indicating strong stability. Strengthening the protection and management of carbon sink core areas is therefore of critical importance for achieving the "dual carbon" goals.

Author Contributions: All authors contributed to the work. N.Z.: Conceptualization, Methodology, Formal analysis, Writing—review and editing, Data curation, Visualization, Investigation, Writing—original draft; Y.C.: Conceptualization, Funding acquisition; J.W.: Writing—review & editing; X.G.: Data curation, Visualization; Y.X.: Methodology, Formal analysis, Writing—review & editing. All authors have read and agreed to the published version of the manuscript.

Funding: This research was funded by National Natural Science Foundation of China, grant number: 52579016, 52379021.

Data Availability Statement: Data will be made available on request.

Conflicts of Interest: The authors declare that they have no known competing financial interests or personal relationships that could have appeared to influence the work reported in this paper.

References

1. Piao, S.; Fang, J.; Ciais, P.; Peylin, P.; Huang, Y.; Sitch, S.; Wang, T. The Carbon Balance of Terrestrial Ecosystems in China. *Nature* **2009**, *458*, 1009–1013. [CrossRef]
2. Wang, T.Y.; Yue, W.Z.; Huang, B.; Zhong, P.Y. Estimation of terrestrial ecosystem carbon sinks and identification of carbon sink conservation areas under future climate change scenarios: A case study of Zhejiang province. *Acta Geogr. Sin.* **2025**, *80*, 183–199. (In Chinese)
3. Smith, P.; Bhogal, A.; Edgington, P.; Black, H.; Lilly, A.; Barraclough, D.; Worrall, F.; Hillier, J.; Merrington, G. Consequences of Feasible Future Agricultural Land-use Change on Soil Organic Carbon Stocks and Greenhouse Gas Emissions in Great Britain. *Soil Use Manag.* **2010**, *26*, 381–398. [CrossRef]
4. Lai, L.; Huang, X.J. (Eds.) *Research on the Carbon Emission Effects of Land Use in China*, 1st ed.; Nanjing University Series on Human Geography; Nanjing University Press: Nanjing, China, 2011. (In Chinese)
5. Houghton, R.A. Revised Estimates of the Annual Net Flux of Carbon to the Atmosphere from Changes in land use and Land Management 1850–2000. *Tellus B* **2003**, *55*, 378–390. [CrossRef]
6. National Remote Sensing Centre Ministry of Science and Technology of the People's Republic of China Global Ecosystems and Environment Research Cooperation. Available online: https://noda.ac.cn/geoarc/2023/index.html (accessed on 11 March 2026). (In Chinese)
7. Zhang, Y.; Chen, W.X.; Wang, G.Z.; Wu, J.H.; Zeng, J.; Liu, Z.L. Multi-scenario simulation of ecosystem services trade-offs and synergies in Chinese urban agglomerations. *China Environ. Sci.* **2025**, *45*, 5742–5755. (In Chinese) [CrossRef]
8. Zhao, M.S.; Wu, T.; Sheng, Y.; Chen, X.J.; Zhang, D.Y.; Lu, Y.Y. Spatial Optimization Simulation of land use in Anhui Province Under the "Dual Carbon Goals". *Environ. Sci.* **2025**, 1–23. [CrossRef]
9. Cai, M.Z.; Xin, X.B.; Pei, S.X.; Wu, S.; Wu, D.; Guo, H. Spatiotemporal dynamic changes and driving forces of forest NPP in Beijing. *Trans. Chin. Soc. Agric. Eng.* **2025**, *41*, 282–290. (In Chinese)
10. Wu, A.B.; Chen, F.G.; You, H.Z.; Zhao, Y.X. Characterization of Spatial and Temporal Changes in Net Primary Productivity of Vegetation in Beijing-Tianjin-Hebei Region and Analysis of Influencing Factors. *Environ. Sci.* **2025**, *46*, 6957–6968. [CrossRef]
11. Ministry of Ecology and Environment of the People's Republic of China. *Technical Guidelines for the Delineation of National Ecological Protection Red Lines*; Ministry of Ecology and Environment of the People's Republic of China: Beijing, China, 2017. (In Chinese)
12. Ministry of Ecology and Environment of the People's Republic of China Technical Specification for Supervision of Ecological Conservation Redline—Baseline Investigation (on Trial). Available online: https://www.mee.gov.cn/ywgz/fgbz/bz/bzwb/stzl/202011/t20201127_810247.shtml (accessed on 11 March 2026). (In Chinese)
13. Ministry of Environmental Protection National Development and Reform Commission Guidelines for the Delineation of China's Ecological Protection Red Lines. Available online: https://www.mee.gov.cn (accessed on 11 March 2026). (In Chinese)
14. Ministry of Natural Resources; Ministry of Ecology and Environment. Notice of the National Forestry and Grassland Administration on Strengthening the Management of Ecological Protection Red Lines (Trial). Available online: https://www.mee.gov.cn/xxgk2018/xxgk/xxgk10/202208/t20220822_992127.html?utm_source=chatgpt.com (accessed on 10 April 2026). (In Chinese)
15. Lv, Q.; Luo, Y.; Gao, Z.; Lei, X. Spatio-temporal Pattern, Dynamic Evolution, and Carbon Compensation Zoning of land use Carbon Budget in Beijing-Tianjin-Hebei Region. *J. Environ. Sci.* **2026**, *47*, 843–854. [CrossRef]
16. Zhang, L.; Jing, C.; Wu, S.; Zhou, Y.; Fang, Z. Evolution of spatial correlation and scenario prediction of land use carbon in the Beijing-Tianjin-Hebei Region. *Sci. Surv. Mapp.* **2025**, *50*, 142–151. (In Chinese) [CrossRef]
17. Chen, J.; Zhang, J.; Li, J.; Li, S. Evolution of spatial correlation and scenario prediction of land use carbon emissions in the Beijing-Tianjin-Hebei Region. *Acta Ecol. Sin.* **2024**, *44*, 2270–2283. (In Chinese) [CrossRef]
18. Du, P.H. *Research on the Carbon Emission Input-Output Model of Beijing-Tianjin-Hebei*; Capital University of Economics and Business: Beijing, China, 2020. (In Chinese)
19. Liang, X.; Guan, Q.; Clarke, K.C.; Liu, S.; Wang, B.; Yao, Y. Understanding the Drivers of Sustainable Land Expansion Using a Patch-Generating land use Simulation (PLUS) Model: A Case Study in Wuhan, China. *Comput. Environ. Urban Syst.* **2021**, *85*, 101569. [CrossRef]
20. Chardon, V.; Herrault, P.; Staentzel, C.; Skupinski, G.; Finance, O.; Wantzen, K.; Schmitt, L. Using Transition Matrices to Assess the Spatio-temporal Land Cover and Ecotone Changes in Fluvial Landscapes from Historical Planimetric Data. *Earth Surf. Process. Land.* **2022**, *47*, 2647–2659. [CrossRef]
21. Xu, X.; Kong, W.; Wang, L.; Wang, T.; Luo, P.; Cui, J. A Novel and Dynamic land use/Cover Change Research Framework Based on an Improved PLUS Model and a Fuzzy Multi objective Programming Model. *Ecol. Inform.* **2024**, *80*, 102460. [CrossRef]

22. Wei, Y.; Zhou, P.; Zhang, L.; Zhang, Y. Spatio-Temporal Evolution Analysis of land use Change and Landscape Ecological Risks in Rapidly Urbanizing Areas Based on Multi-Situation Simulation—A Case Study of Chengdu Plain. *Ecol. Indic.* **2024**, *166*, 112245. [CrossRef]
23. Liu, J.; Liu, B.; Wu, L.; Miao, H.; Liu, J.; Jiang, K.; Ding, H.; Gao, W.; Liu, T. Prediction of land use for the next 30 Years Using the PLUS Model's Multi-Scenario Simulation in Guizhou Province, China. *Sci. Rep.* **2024**, *14*, 13143. [CrossRef] [PubMed]
24. Chang, S.P. *Land Use Change, Simulation and Prediction Study in the Ecological Conservation Area of Northwestern Beijing*; Beijing Forestry University: Beijing, China, 2021. (In Chinese)
25. Wu, C.; Chen, B.; Huang, X.; Dennis Wei, Y.H. Effect of land use Change and Optimization on the Ecosystem Service Values of Jiangsu Province, China. *Ecol. Indic.* **2020**, *117*, 106507. [CrossRef]
26. Li, P.R.; Wang, X.J.; Xu, S.X.; Gao, S.H.; Xue, Z.X.; Heng, R. Spatiotemporal pattern of NEP in Aksu River Basin based on PLUS land use simulation. *Arid Zone Res.* **2024**, *41*, 1059–1068. (In Chinese) [CrossRef]
27. Potter, C.; Klooster, S.; Huete, A.; Genovese, V. Terrestrial Carbon Sinks for the United States Predicted from MODIS Satellite Data and Ecosystem Modeling. *Earth Interact.* **2007**, *11*, 1–21. [CrossRef]
28. Zhu, W.Q.; Pan, Y.Z.; Zhang, J.S. Estimation of Net Primary Productivity of Chinese Terrestrial Vegetation Based on Remote Sensing. *J. Plant Ecol.* **2007**, *03*, 413–424. (In Chinese)
29. Odum, H.T. Primary Production in Flowing Waters1. *Limnol. Oceanogr.* **1956**, *1*, 102–117. [CrossRef]
30. Woodwell, G.M.; Whittaker, R.H. Primary Production in Terrestrial Ecosystems. *Am. Zool.* **1968**, *8*, 19–30. [CrossRef]
31. Moran, P.A.P. The Interpretation of Statistical Maps. *J. R. Stat. Soc. Ser. B Stat. Methodol.* **1948**, *10*, 243–251. [CrossRef]
32. Thomson, R.; Espin, J.; Samuels-Jones, T. Green Crime Havens: A Spatial Cluster Analysis of Environmental Crime. *Soc. Sci. Q.* **2020**, *101*, 503–513. [CrossRef]
33. Getis, A.; Ord, J.K. The Analysis of Spatial Association by Use of Distance Statistics. *Geogr. Anal.* **1992**, *24*, 189–206. [CrossRef]
34. Zeng, J.; Wu, J.; Chen, W. Coupling Analysis of land use Change with Landscape Ecological Risk in China: A Multi-Scenario Simulation Perspective. *J. Clean. Prod.* **2024**, *435*, 140518. [CrossRef]
35. Li, C.; Gao, B.; Wu, Y.; Zheng, K.; Wu, Y. Dynamic simulation of landscape ecological risk in mountaintowns based on PLUS model. *J. Zhejiang AF Univ.* **2022**, *39*, 84–94. (In Chinese) [CrossRef]
36. Chen, F.; Guo, A.; Wu, A.; Wang, Y.; Fan, J. Evolution of Urban Expansion Pattern and Its Impact on the Quality of the Ecological Environment in the Beijing-Tianjin-Hebei Urban Agglomeration. *Environ. Sci.* **2025**, *46*, 3708–3719. (In Chinese) [CrossRef]
37. Zeng, L.; Yang, L.; Su, L.; Hu, H.; Feng, C. The Impact of Policies on land use and Land Cover Changes in the Beijing–Tianjin–Hebei Region in China. *Environ. Impact Assess. Rev.* **2025**, *110*, 107676. [CrossRef]
38. Guan, Y.; Wang, J.; Tan, L.; Yang, S.; Zhao, W.; Chen, K.; Zhang, X. Estimation of Vegetation Carbon Source/sink and Its Response to land use Change in the Loess Plateau, a Case Study of Yanhe River Basin. *Environ. Sci.* **2025**, *46*, 1657–1665. (In Chinese) [CrossRef]
39. Xiong, Z.; Li, S.; Liu, Q.; Zhang, H.; Cai, Y. Spatial characteristics and influencing factors of urban net carbon sinks in China. *J. Environ. Eng. Technol.* **2026**, *16*, 54–66. (In Chinese)
40. Lu, Y.; Li, X.; Zhao, H.; Han, C.; Liu, X.; Mao, J. Spatial heterogeneity of forest ecosystem services and influencing. *J. Beijing Norm. Univ. (Nat. Sci.)* **2024**, *60*, 350–357. (In Chinese)
41. Liu, M.; Li, G.; Ren, X. Advances in Research on Carbon and Water Flux in Farmland Ecosystem. *J. Henan Univ. (Nat. Sci.)* **2021**, *51*, 253–267. (In Chinese) [CrossRef]
42. Ma, Z.; Cui, H.; Ge, Q. Prediction of net primary productivity change pattern in China based on vegetation dynamic models. *J. Geogr.* **2022**, *77*, 1821–1836. (In Chinese)

Disclaimer/Publisher's Note: The statements, opinions and data contained in all publications are solely those of the individual author(s) and contributor(s) and not of MDPI and/or the editor(s). MDPI and/or the editor(s) disclaim responsibility for any injury to people or property resulting from any ideas, methods, instructions or products referred to in the content.